Chemical Physics Letters 531 (2012) 18–21

Contents lists available at SciVerse ScienceDirect

Chemical Physics Letters

journal homepage: www.elsevier.com/locate/cplett

Energetic ballistic deposition of volatile gases into ice

K.D. Gibson, Daniel R. Killelea [1], James S. Becker [2], Hanqiu Yuan, S.J. Sibener *

The James Franck Institute and Department of Chemistry, The University of Chicago, 929 East 57th Street, Chicago, IL 60637, USA

ARTICLE INFO

Article history:
Available online 20 February 2012

ABSTRACT

Gases are trapped in ice when they adsorb to the surface and are subsequently buried by further adsorption of water. Low surface temperatures, where the surface residence time of the gas is long, are needed to permit burial. Here, we demonstrate a new mechanism, energetic ballistic deposition, which has not been previously reported. Translationally energetic xenon atoms penetrate the ice surface and become stably embedded within the ice well above the xenon desorption temperature. This new mechanism for gaseous incorporation warrants consideration in models that seek to accurately describe the trapping and concentration of volatile gases in molecular solids.

The trapping of volatile gases within ice plays a key role in the formation of heterogeneous icy planetesimals and is the primary method for preconcentration of reagents in the formation of complex molecules in the extraterrestrial environment [1–3]. Moreover, because volatile species trapped in ice play a central role in determining the composition of planetary atmospheres, a thorough understanding of the microscopic steps in their formation is necessary for the development of accurate models of atmospheric and extraterrestrial systems [4–8]. In general, volatile species are trapped in an ice when they adsorb to the ice surface for sufficient time to allow for more gas-phase water to condense, thus preventing the volatile species from desorbing back into the gas phase. Because surface residence time is highly dependent on the temperature of the ice, low temperatures (<100 K) are typically required to adsorb an appreciable amount of volatile species [9,10]. Alternatively, volatiles may be stabilized in an ice at somewhat higher temperatures by the formation of clathrates [9,11,12]. Clathrates are distinct species in which the host ice forms a highly stable, cage-like structure around the volatile species, trapping them in the matrix. However, under the low pressure conditions typical of astrophysical environments, clathrates of xenon and water ice decompose at temperatures near 60 K [11]. The processes for trapping volatiles in ices thus far considered represent systems formed at thermal equilibrium, where thermodynamics determines the composition of the ice and the amount of volatile species embedded in the matrix.

In this Letter, we turn our attention to the high-energy collisions of neutral xenon with non-porous amorphous or crystalline ice surfaces. In the laboratory frame of reference, xenon atoms with 6.5 eV of translational energy collided with a stationary ice surface at a speed of 3.1 km s^{-1}. The relative velocities of these collisions are well within the range of collisional speeds between gas atoms and icy planetesimals in interplanetary space [13,14]. We show that at these high translational energies, a small but clearly discernable number of the xenon atoms become embedded and remain absorbed within the ice structure. Importantly, this process occurs at ice temperatures greater than 110 K, significantly above the 55 K desorption temperature of xenon adsorbed on ice [15] or the near 60 K decomposition temperature of xenon–ice clathrates [11]. Rather than being adsorbed and then buried as further water is condensed, the xenon is directly implanted, and this process can occur at elevated ice temperatures.

These observations clearly establish a high-energy embedding process as an important mechanism for the formation of heterogeneous icy species under conditions relevant to those found in interplanetary space. There is some precedent for this process, Daschbach et al. implanted helium into ultrathin ice films at 25 K [16], but those results were for unique ice structures on Pt(1 1 1) at exceedingly low temperatures. Argon and other low-boiling gases can be trapped in highly porous amorphous solid water. The condensed gases may then diffuse into the bulk of the ice [17]. There are two key distinctions between these previous experiments and the results presented herein. The collision energies of the incident species studied here using a supersonic beam source cover the range between 1.7 and 6.5 eV, whereas in the previous work a thermal source was used, leading to gas-surface collision energies of at most a few tenths of an eV. Moreover, we found that xenon is directly injected into the ice as a consequence of the high energy collision, rather than first being adsorbed and percolating into pores or being buried by the condensation of additional water. The xenon embedding process depends strongly on the incident angle (Θ_I) of the xenon atoms and their translational energy (E_I).

* Corresponding author.
E-mail address: s-sibener@uchicago.edu (S.J. Sibener).
[1] Present address: Loyola University Chicago, Department of Chemistry, 1068 W. Sheridan Rd., Chicago, IL 60660, USA.
[2] Present address: Intel Corporation, Hillsboro, OR, USA.

0009-2614/$ - see front matter © 2012 Elsevier B.V. All rights reserved.
doi:10.1016/j.cplett.2012.02.040

Additionally, we present data that show that the xenon that did not embed, but rather scattered from the ice surface, has lost most of its initial translational energy.

The experiments were performed using a precision ultra-high vacuum (UHV) gas-surface scattering instrument (base pressure 1×10^{-10} Torr) that is capable of having up to three independent molecular or atomic beams impinging simultaneously on a target Rh(1 1 1) crystal [18]. The Rh(1 1 1) was resistively heated and cooled with liquid nitrogen. The sample mount could be rotated with respect to the incident beams allowing for a range of different Θ_I to be studied. The angular dependencies of the final energy (E_F) and intensity of xenon scattered from the surface were measured with a doubly-differentially pumped quadrupole mass spectrometer (QMS) that could be independently rotated around the target crystal.

Molecular beam techniques were used to prepare intense beams of xenon atoms with a narrow (c.a. 10% ΔE_I (FWHM)/E_I) distribution of translational energy. High velocity beams of xenon atoms were formed through a supersonic expansion of dilute mixtures of xenon (1% Xe) in lighter carrier gases. Under these conditions, the heavier xenon atoms have nearly equivalent velocities as the lighter carrier gas, either He or H_2. The energy of the xenon atoms in the beam was tuned between 1.1 and 6.5 eV by varying the carrier gas and the nozzle temperature (323–673 K). The xenon beams were made by expanding the gas mixture through a heatable nozzle with a 20 μm pinhole at a few hundred psi backing pressure. Time-of-flight analysis of the incident xenon beams determined the energy distribution and relative flux. The absolute xenon fluxes on target were on the order of 10^{15} Xe cm^{-2} s^{-1} at normal incidence [19].

Icy particles are formed in space through aggregation of gas-phase species and thus are likely a mixture of small domains of amorphous solid water and crystalline ice [3]. Amorphous solid water (ASW) is a molecularly disordered, metastable phase of ice formed by vapor deposition at temperatures below 120 K. Crystalline ice (CI) is the ordinary hexagonal ice phase and is formed at temperatures of 140 K or higher. To avoid any influence on the ice morphology by the underlying metal substrate, ice films of at least 1000 layers thickness were grown. D_2O was used in these studies because the background signal in the detector at m/e = 20 (D_2O^+) was much smaller than at m/e = 18 (H_2O^+), leading to greater sensitivity for detecting sputtered molecules, a related experiment not discussed here [20]. Both the crystalline and amorphous ices grown lack any long range order at these thicknesses and the Rh(1 1 1) substrate does not affect the nature of the ice film [21]. To further ensure this lack of long-range order, the Rh(1 1 1) surface was predosed with O_2 to create an ordered 0.5 monolayer O structure [22]. Ice films were then grown by dosing the prepared substrate with D_2O from a molecular beam produced by bubbling He through a D_2O filled reservoir. The ice was deposited at a rate of 0.5 layers s^{-1} (1 layer = 1.07×10^{15} D_2O cm^{-2}). The use of D_2O from a molecular beam minimizes background accumulation typically encountered when backfilling a vacuum chamber with water vapor and allows for the deposition of high-purity ice films of known morphology; the morphology of the ice (ASW or CI) depends on the temperature of the Rh(1 1 1) substrate during deposition. Film thickness was determined by temperature programmed desorption (TPD), where the surface temperature was ramped while monitoring the D_2O signal. The coverage calibration was done by comparing the post-exposure TPD signal with that of a monolayer of D_2O [22]. The shape of the TPD spectra verified whether the ice overlayer was CI or ASW, where the desorption of crystalline ice is a smooth peak and there is a small bump in the desorption peak near 160 K for amorphous solid water [23]. The lack of long-range surface ordering was verified using helium atom scattering, where a 19 meV He beam probed the surface order. No elastic diffraction features, not even a specular scattering peak, were observed. The ice was likely composed of many individual grains that were not azimuthally aligned, and the surface was not atomically flat, a good model for naturally occurring ice. Highly porous ices are grown at very low deposition temperatures (<70 K), but at the deposition temperature employed in this study, 120 K for ASW and 140 K for CI, the surface was not porous [24–26]. For both ASW and CI, once the ice film was prepared, it was cooled to 120 K for exposure to xenon atoms. In other measurements, we also cooled ice films to ~50 K, and then exposed them to a low energy Xe beam (~63 meV), and there was a single Xe TPD peak at ~70 K, suggesting that the atoms are only adsorbed on the surface.

The ice was exposed to a continuous beam of xenon atoms of a selected translational energy and incident angle while using the rotatable detector to make TOF measurements of the scattered xenon at various final angles (Θ_F). The translational energy distribution of the scattered xenon atoms was derived from the collected TOF spectra. A representative distribution is shown in the inset of Figure 1. The bimodal distribution is a clear signature of the xenon scattering through two separate scattering processes. The first feature is lower energy, arising from xenon atoms that were transiently trapped on the ice surface, reached thermal equilibrium with the surface and subsequently desorbed. This process, trapping-desorption (TD), is well described by a Maxwell–Boltzmann distribution with an average energy of $2k_BT_{ice}$, where T_{ice} is the temperature of the ice surface, here 120 K, $\langle E \rangle$ = 0.02 eV, and k_B is Boltzmann's constant. The second feature is higher energy, or faster, xenon atoms that scattered from the surface with significant energy loss, but were not thermally equilibrated with the surface. These atoms are well represented by a shifted Maxwell–Boltzmann distribution with an average energy of close to 0.2 eV. The shifted Maxwell–Boltzmann distributions are flexible distributions that are often employed in scattering measurements, and provide a quantitative handle for discussion of the relative energies of the two ensembles of xenon atoms. Although almost all of the

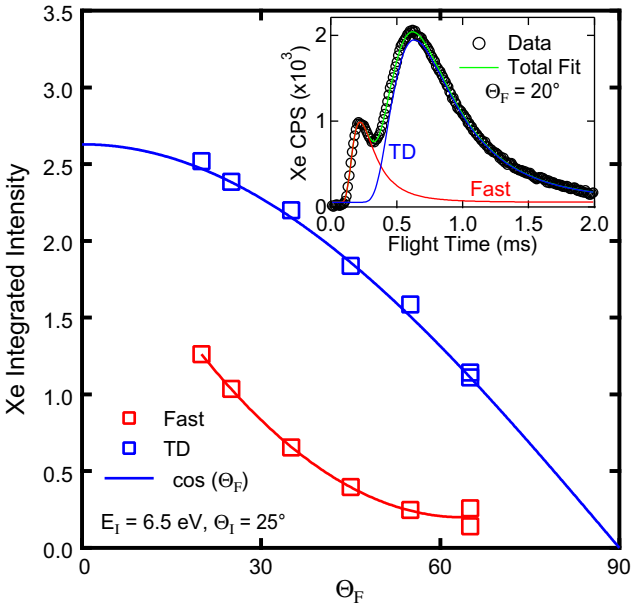

Figure 1. Angular dependence of the intensity of xenon scattered via the fast channel (red) and the trapping-desorption channel (blue). The solid line through the trapping-desorption data is a cos(Θ_F) least squares fit, and the solid line through the fast data is simply to guide the eye. The inset shows an example of the time of flight distribution. The data are open circles, and the total fit is the solid green line. The fits for the fast and TD channels are shown in red and blue, respectively. The conditions were: E_I = 6.5 eV, Θ_I = 25°, and ASW ice at T_S = 115 K.

scattered xenon atoms' initial energy was dissipated to the ice lattice, their final energy was still significantly greater than the scattered atoms from the trapping-desorption channel. Figure 1 shows the relative intensity of the two scattering channels at various final scattering angles for 6.5 eV xenon atoms impinging at 25° on ASW. The scattering was qualitatively similar for CI under the same conditions. Each data point was derived by integrating the energy distribution (as shown in the inset of Figure 1) of the scattered xenon at a given exit angle (Θ_F). As Θ_I becomes more glancing, the faster scattering component becomes more energetic and intense relative to the slower trapping-desorption channel. Under all conditions, an appreciable trapping-desorption scattering component was observed.

After exposing the ice sample to a beam of energetic xenon, TPD experiments that measured both the desorbing xenon ($m/e \approx 132$) and D_2O were performed on the resultant ice film. Figure 2 shows plots of post-exposure TPDs comparing xenon desorption from either ASW (blue) or CI (red) after exposure to 6.5 eV xenon atoms at normal incidence. For the TPD plots, the ordinate scaling is the measured TPD signal divided by the relative xenon flux of the incident beam (as measured by TOF spectra), the exposure time, and $\cos(\Theta_I)$. This is called the exposure weighted xenon TPD signal. The total exposure was nearly 8% larger for the ASW than for the CI. As shown in the figure, there are unmistakable xenon desorption peaks nearly 100 K above the expected desorption temperature (55 K) for xenon on ice [9,11,12]. Furthermore, the desorption temperature is different for each ice morphology. On crystalline ice, xenon desorbs as a single peak near 140 K and desorption of xenon is complete before any significant desorption of the ice occurs; crystalline D_2O desorption is shown by the thin dashed line in Figure 2. Xenon desorption from ASW has a more complicated profile comprised of two separate xenon desorption peaks. The first peak is qualitatively similar to desorption from CI, but shifted about 15 K higher. The second is a sharp peak near 160 K. ASW irreversibly converts to CI around 160 K [23], and is evident as a hump in the D_2O desorption indicated by the thin solid black line in Figure 2. A significant amount of the desorbing xenon came off as a sharp feature near this transition, which we attribute to long-range diffusion followed by the expulsion of the xenon as the ice crystallizes [27].

Figure 3 shows the exposure weighted xenon TPD spectra from ASW after exposure to beams of xenon atoms of different incident energies and angles. The total xenon fluences for each exposure were within a factor of 1.5, and this small deviation in total exposure had no apparent effect on the TPD peak shape or intensity. As can be seen in the figure, at the lowest E_I and glancing incidence, no xenon was measured in the TPD. As E_I increased at 25° incidence, a sharp desorption feature grew near 160 K. Finally, at the greatest E_I studied, a second, broader peak developed below 155 K. Taken together, these results show that the amount of embedded xenon increases with greater E_I and more normal incidence. The data in Figure 3 suggest that embedding is increasingly favored with higher incident energy, and therefore higher incident momentum. One consequence of this trend would be that embedding of heavy atoms would be favored over light atoms having the same energy (and commensurately lower momentum). The effect that momentum has on embedding of the incident gas atoms will be discussed in an forthcoming publication.

The presence of the trapping desorption channel in the scattering (Figure 1) suggests that the xenon has a significant residence time on the ice surface. While adsorbed to the surface, it is possible that the xenon could diffuse into the ice bulk. Because no xenon was observed to embed under the gentlest conditions (low E_I and glancing incidence), where there is an appreciable TD component, diffusion from the surface into the bulk is not an important contribution to the embedded xenon observed after more vigorous exposures.

It is important to explain why the ordinate is scaled by the xenon exposure rather than just showing the absolute signal. The xenon is trapped within the ice, so it is reasonable that there be a limit to how much xenon can be adsorbed at any depth below the ice surface. The penetration and embedding involve the breaking and reformation of many intermolecular D_2O bonds, which

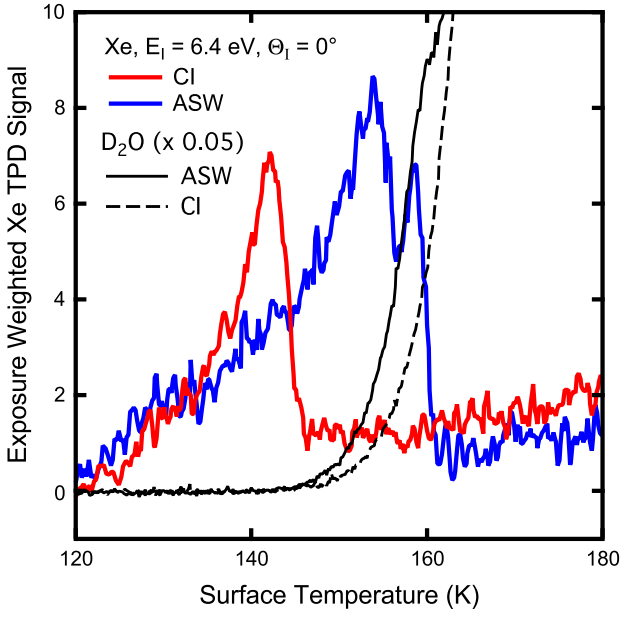

Figure 2. Exposure weighted TPD spectra (10 K min^{-1} ramp rate) for xenon desorbing from either crystalline ice (CI, red) or ASW (blue). Both substrates were exposed to a 6.4 eV xenon beam at normal incidence for nearly the same xenon exposure (about 8% difference). The scaled (divided by 20) D_2O desorption spectra are shown for CI (dashed) and ASW (solid). The ASW to CI transition is shown by the hump in the ASW desorption around 160 K which is coincident with the second xenon desorption.

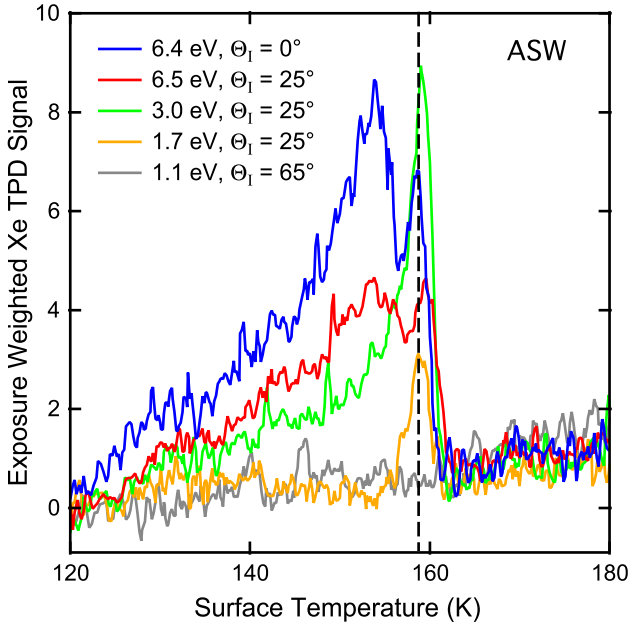

Figure 3. Exposure weighted TPD spectra (10 K min^{-1} ramp rate) for xenon desorbing from ASW after several different dose conditions. The 6.4 eV, normal incidence data are the same as shown in Figure 2 and the dashed vertical line corresponds to the ASW-CI transition near 160 K. The xenon TPD spectrum for 1.7 eV at 65° incidence (gray line) establishes the background xenon signal, as no xenon was observed.

have an energy of about 0.3 eV per bond [28]. Higher energy xenon can penetrate deeper into the ice, leading to a larger quantity of xenon incorporated in the ice matrix. At more glancing incident angles, the impinging xenon atom would encounter many more D_2O molecules to reach a given depth below the surface than if it struck the surface at 0°. The incident xenon loses energy with each encounter, so it would be expected that for a given E_I, less would be adsorbed with increasing Θ_I. With this interpretation, there should be a saturation limit for any given E_I and Θ_I; the amount of xenon adsorbed should at first increase with continued exposure, but eventually reach a limit. The experiments discussed in this Letter do not address the uptake kinetics of the embedding process, but we are presently conducting experiments that will, and these will be presented in a future publication.

In conclusion, we have shown that xenon atoms can be embedded in amorphous and crystalline ice at hyperthermal incident energies and near-normal incident angles. Most importantly, the gas embedding occurs at temperatures (120 K) well above the normal desorption temperature of xenon adsorbed on the ice surface (55 K). These results demonstrate a new mechanism for the incorporation of gaseous moieties in the surface region of both amorphous solid water and crystalline ice. This uptake mechanism has not been previously considered as a route by which icy planetesimals in interplanetary or interstellar space can acquire new material in the astrophysical environment.

Acknowledgments

This work was supported by the National Science Foundation CCI Center for Energetic Non-Equilibrium Chemistry at Interfaces (CENECI), Grant No. 0943639. Seed funding and instrumentation support is also gratefully acknowledged from the Air Force Office of Scientific Research and DTRA (Grant No. HDTRA1-11-1-0001).

References

[1] B.M. Jones, F. Zhang, R.I. Kaiser, A. Jamal, A.M. Mebel, M.A. Cordiner, S.B. Charnley, Proc. Natl. Acad. Sci. USA. 108 (2011) 452.
[2] P. Ehrenfreund, S.B. Charnley, Annu. Rev. Astron. Astrophys. 38 (2000) 427.
[3] P. Jenniskens, D.F. Blake, Science 265 (1994) 753.
[4] A. Bar-Nun, G. Notesco, T. Owen, Icarus 190 (2007) 655.
[5] D.J. Burke, W.A. Brown, Phys. Chem. Chem. Phys. 12 (2010) 5947.
[6] T. Owen, Space Sci. Rev. 138 (2008) 301.
[7] T. Owen, A. Bar-Nun, Icarus 116 (1995) 215.
[8] W. Whiston, A New Theory of the Earth, From its Original to the Consummation of All Things, Cambridge University Press, London, 1738.
[9] N. Iro, D. Gautier, F. Hersant, D. Bockelee-Morvan, J.I. Lunine, Icarus 161 (2003) 511.
[10] G. Notesco, A. Bar-Nun, T. Owen, Icarus 162 (2003) 183.
[11] D. Gautier, F. Hersant, Space Sci. Rev. 116 (2005) 25.
[12] J.I. Lunine, D.J. Stevenson, Astrophys. J. Suppl. Ser. 58 (1985) 493.
[13] L.L. Hood, Meteorit. Planet. Sci. 33 (1998) 97.
[14] J.K. Baird, J. Spacecraft Rockets 35 (1998) 62.
[15] A.P. Graham, J.P. Toennies, J. Chem. Phys. 118 (2003) 2879.
[16] J.L. Daschbach, G.K. Schenter, P. Ayotte, R.S. Smith, B.D. Kay, Phys. Rev. Lett. 92 (2004) 198306.
[17] D. Laufer, E. Kochavi, A. Bar-Nun, Phys. Rev. B 36 (1987) 9219.
[18] N. Isa, K.D. Gibson, T. Yan, W. Hase, S.J. Sibener, J. Chem. Phys. 120 (2004) 2417.
[19] D R Killelea, H Yuan, J S Becker, K D Gibson, S J Sibener, Submitted.
[20] K.D. Gibson, D.R. Killelea, S.J. Sibener, J. Phys. Chem. C 113 (2009) 13325.
[21] R.S. Smith, C. Huang, E.K.L. Wong, B.D. Kay, Surf. Sci. 367 (1996) L13.
[22] K.D. Gibson, M. Viste, S.J. Sibener, J. Chem. Phys. 112 (2000) 9582.
[23] R.J. Speedy, P.G. Debenedetti, R.S. Smith, C. Huang, B.D. Kay, J. Chem. Phys. 105 (1996) 240.
[24] D.E. Brown, S.M. George, C. Huang, E.K.L. Wong, K.B. Rider, R.S. Smith, B.D. Kay, J. Phys. Chem. 100 (1996) 4988.
[25] K.P. Stevenson, G.A. Kimmel, Z. Dohnalek, R.S. Smith, B.D. Kay, Science 283 (1999) 1505.
[26] G.A. Kimmel, K.P. Stevenson, Z. Dohnalek, R.S. Smith, B.D. Kay, J. Chem. Phys. 114 (2001) 5284.
[27] R.S. Smith, C. Huang, B.D. Kay, J. Chem. Phys. B 101 (1997) 6123.
[28] V.F. Petrenko, R.W. Whitworth, Physics of Ice, Oxford University Press, Oxford, 1999.